Fractional Revivals in Elliptical Atomtronics

Sriganapathy Raghav[1], Suranjana Ghosh[2], Luca Salasnich[3], Jayanta Bera[4], and Utpal Roy[1]*
[1]*Indian Institute of Technology Patna, Bihta, Patna-801106, India*
[2]*Indian Institute of Science Education and Research Kolkata, West Bengal, India*
[3] *Dipartimento di Fisica e Astronomia "Galileo Galilei", Universitá di Padova, Via Marzolo 8, 35131 Padova, Italy*
[4] *C. V. Raman Global University, Bhubaneswar, Odisha-752054, India*

Fractional revivals are recently reported for circular atomtronics, but get disturbed for a nonzero eccentricity of the waveguide geometry. Here, we provide a mechanism for the elliptical atomtronics with arbitrary eccentricity to restore fractional revivals. The uniform ground state of the circular waveguide becomes nonuniform in the elliptical geometry. An appropriate dispersion management can bring back the uniformity and we use the overlap function numerically to identify the corresponding dispersion coefficients, which match with our proposed analytical formula. The fact that, the cloud spends mostly along the semimajor edges, is demonstrated by the survival function. The said dispersion management recovers the desired fractional revivals patterns, where the revival timescale becomes independent of the eccentricity. The present method paves the way also to observe other known phenomena of circular atomtronics in elliptical atomtronics.

I. INTRODUCTION

Guiding matter waves is a pivotal component in constructing matter wave circuits, particularly within atom chip technology [1–3]. The precise fabrication of these waveguides is critical in the field of atomtronics, enabling coherent control and manipulation of matter waves [4, 5]. Techniques like time-averaged adiabatic potential (TAAP) [6–10], intensity mask [11], and digital holography [12] have been instrumental in creating waveguides for ultracold atoms, contributing significantly to the advancement of atomtronics. Among the various types of waveguides, the circular waveguide stands out as the simplest spatially closed atomtronic circuit [13, 14], widely applied in atom interferometry [15–19], quantum transport [20, 21], quantum sensing [22–24], atom SQUID [25, 26], and other quantum technological applications [2]. The curvature-induced potential (CIP) of a waveguide is proportional to the square of its curvature, implying a constant CIP for a circular waveguide [27–29], which bears a uniformly distributed ground state along its circumference [30].

The major utility of a circular waveguide stems from its constant curvature, which facilitates matter wave interference, an integral component of the above applications. The matter wave interference in a circular waveguide also gives rise to fractional revivals (FR), which is the spawning of multiple replicas of the initial matter wave packet along the perimeter of the circular waveguide [31–33]. The FR instances are succeeded by the revival of the initial condensate in shape and location. The FR time instances and revival depends on a characteristic parameter linked to the radius of the waveguide [32]. Moreover, higher-order FR patterns can provide a platform for studying multiple source interference, which is usually studied using optical lattices [34–37]. In contrast, due to the variable width along the circumference and non-constant CIP, elliptical waveguides result in a non-uniform ground state along the perimeter [30, 38]. Unlike a circular waveguide, elliptical counterpart lacks support for Talbot oscillations [39].

Concurrently, dispersion engineering has emerged as a significant method for controlling and manipulating the dynamics of Bose-Einstein condensates (BEC) in external traps [40–42]. Dispersion management (DM) in atomic BECs is achieved by introducing optical lattices [43, 44] or manipulating spin-orbit coupling [45, 46]. One can achieve desired BEC dynamics in a matter-wave circuit of waveguides by tuning the nonlinearity and the dispersion through Feshbach resonance and DM, as in the case of optical solitons [47, 48]. Recently, the nonlinearity of the BEC was used to nullify the effects of curvature in an elliptical waveguide [38]. Here, we delve into engineering the dispersion of BEC inside an elliptical waveguide to regain the properties of circular atomtronics. Notably, the utilization of matter wave dispersion serves as a means to counteract the effects of non-constant width in an elliptical waveguide, offering potential strategies for manipulating and optimizing matter wave behaviour in atomtronics applications.

The paper is organized as follows: Section II introduces the theoretical model for BEC in an elliptical waveguide. This section also discusses the role of waveguide geometry in the dispersion of matter waves. In Sec. III, we derive the dynamical equation for BEC with tunable dispersion in an elliptical waveguide and also outline the numerical methods applied to obtain both the ground state solution and FR-dynamics within the waveguide. The ground state solution of BEC in an elliptical waveguide, characterized by different eccentricities, are demonstrated. We also determine the suitable dispersion coefficients for matter waves, aiming to neutralize the effects of variable thickness in an elliptical waveguide. Section IV delves into exploring the impact of eccentricity on

* uroy@iitp.ac.in

the FR-dynamics of matter waves and the subsequent restoration of FR signatures through dispersion management, which elucidates on how manipulating dispersion can counteract the challenges posed by the non-constant width in elliptical waveguides. Finally, we conclude in Sec. V, summarizing the key findings and future outlook.

II. BOSE-EINSTEIN CONDENSATE INSIDE AN ELLIPTICAL WAVEGUIDE

We consider a BEC of N number of ^{23}Na atoms, loaded in an elliptical waveguide of eccentricity ε. A three-dimensional Gross Pitaevskii equation (3D-GPE) [49–53] describes the evolution of the macroscopic wavefunction $\Psi \equiv \Psi(r,t)$ of a BEC in an external trap:

$$i\hbar\frac{\partial\Psi}{\partial t} = \left[-\frac{\hbar^2}{2m}\nabla^2 + \frac{4\pi N a_s}{m}|\Psi|^2 + V(r)\right]\Psi, \qquad (1)$$

where $V(r) = V(z) + V(x,y)$ with $V(z) = \frac{1}{2}m\omega_\perp z^2$ and

$$V(x,y) = V_0\left\{1 - \exp\left[-\frac{1}{\gamma^2}\left(\sqrt{x^2+\frac{y^2}{1-\varepsilon^2}} - a\right)^2\right]\right\}.$$

Here, $\omega_\perp$ is the frequency of the transverse harmonic trap, V_0 is the depth of the waveguide, γ is the width of the waveguide, and $\varepsilon = \sqrt{1-\frac{b^2}{a^2}}$ is the eccentricity. For a circular waveguide with a radius a, we take $\varepsilon = 0$, and for an elliptical waveguide with a semi-major radius a, we consider a non-zero eccentricity.

The 3D GPE in Eq.1 is reduced to effective 2D GPE by considering a strong trap in the transverse direction by writing the wavefunction as $\Psi(r,t) = \psi(x,y,t)\Phi(z)$. Here, the function $\psi(x,y,t)$ describes the dynamics of BEC in the elliptical waveguide and $\Phi(z)$ denotes the ground state of the strong axial trap, which is a Gaussian wavefunction with width $a_\perp$ [54]. The effective 2D GPE in the dimensionless form is obtained after integrating out the z component and by scaling position, time and energy by $a_\perp$, $\frac{1}{\omega_\perp}$ and $\hbar\omega_\perp$, respectively. Here $a_\perp = \sqrt{\frac{\hbar}{m\omega_\perp}}$ and $\omega_\perp$ are the harmonic oscillator length and frequency in the transverse direction, respectively.

$$i\frac{\partial\psi}{\partial t} = \left[-\frac{1}{2}\nabla^2_{x,y} + g|\psi|^2 + V(x,y)\right]\psi \qquad (2)$$

Here, $g = \frac{2\sqrt{\pi}Na_s}{a_\perp}$ and, $V(x,y)$ is the potential of the elliptical waveguide scaled by $\hbar\omega_\perp$. This elliptical waveguide has varying thickness for non-zero eccentricity and manifests nontrivial dynamics.

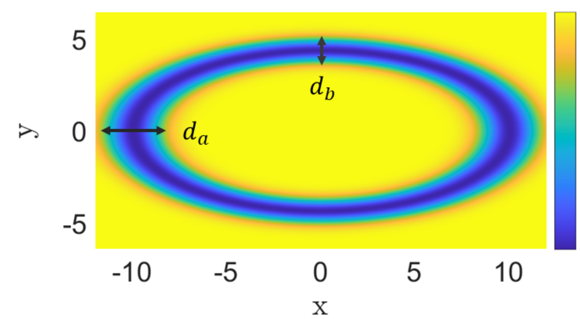

FIG. 1. Elliptical ring trap with varying width along its circumference. The semimajor radius is taken as $a = 10a_\perp$, and the semiminor radius is $b = 4.36a_\perp$. The corresponding eccentricity is $\varepsilon = 0.9$. x and y are in the units of $a_\perp = 2.32\ \mu$m and, t is in the units of $1/\omega_\perp = 1.95$ ms.

A. Waveguide Geometry and Matter Wave Dispersion

A circular waveguide with $\varepsilon = 0$, formed by a ring Gaussian potential, has constant width [55] unlike an elliptical waveguide, as shown in Fig.1. This varying width of the ring affects the dispersion across different waveguide segments. To elucidate the influence of nonzero eccentricity on dispersion, we study the dynamics of a Gaussian wavepacket, placed at two different positions inside the elliptical waveguide, namely $(a,0)$ and $(0,b)$. The wavepacket is expressed as

$$\chi(s,t) = e^{-i\frac{E_k t}{\hbar}}\chi(s,0). \qquad (3)$$

By decomposing the initial wavefunction into its constituent Fourier modes, we write

$$\chi(s,t) = \left(\frac{d}{\sqrt{\pi}}\right)^{\frac{1}{2}}\int_{-\infty}^{\infty}\frac{dk}{\sqrt{2\pi}}e^{-\frac{d^2k^2}{2}}e^{-i\frac{E_k t}{\hbar}}e^{iks}, \qquad (4)$$

where, d is related to the width of the wavepacket, and k relates the energy: $E_k = \hbar^2k^2/(2m)$, which allows us to simplify the wavefunction in Eq.4 as,

$$\chi(s,t) = \left(\frac{D}{\sqrt{\pi}d}\right)^{\frac{1}{2}}e^{-\frac{Ds^2}{2d^2}} \qquad (5)$$

with $D = \frac{1}{(1+i\frac{\hbar t}{md^2})}$. Consequently, the width at time t becomes

$$w_t^2 = \int_{-\infty}^{\infty}\chi^*(s,t)s^2\chi(s,t)ds = w_0^2 + \frac{\hbar^2t^2}{4m^2w_0^2}. \qquad (6)$$

Here, the initial width is given by $w_0 = \frac{d}{\sqrt{2}}$ and the above expression reduces to a dimensionless form as

$$w_t^2 = w_0^2 + \frac{t^2}{4w_0^2}. \tag{7}$$

For analysing the dispersions corresponding to the initial positions, $(a, 0)$ and $(0, b)$, along the elliptical waveguide, we write the respective widths of the waveguide as d_a and d_b, having ratio $\frac{d_b}{d_a} = \sqrt{1-\varepsilon^2}$. An intuitive understanding and numerical trials suggest us to take the transverse widths of the wavepacket as d_a and d_b, respectively, to prevent inhomogeneous dispersion.

Accordingly, the normalization of the wavepacket at these places dictates that their longitudinal widths, w_a and w_b, should be inversely related to d_a and d_b:

$$\frac{w_a}{w_b} = \frac{d_b}{d_a} = \sqrt{1-\varepsilon^2}, \tag{8}$$

which facilitates us to write their relation at time t, following Eq.7 as

$$w_{b,t}^2 = \frac{1}{1-\varepsilon^2}\left[w_a^2 + \frac{t^2(1-\varepsilon^2)^2}{4w_a^2}\right]. \tag{9}$$

It becomes apparent that, the widths of the wavepacket at the semi-major and semi-minor edges deviate from their initial ratio (Eq.8). The factor $(1-\varepsilon^2)^2$ introduces the inhomogeneity of the widths over the time. This demands a modification of E_k by the same factor, such that $E_k = \frac{1}{(1-\varepsilon^2)}\frac{\hbar^2 k^2}{2m}$, to compensate the deviation, caused by the nonzero eccentricity. Hence, the time dependent widths maintain the initial ratio:

$$w_{b,t}^2 = \frac{1}{1-\varepsilon^2}\left[w_a^2 + \frac{t^2}{4w_a^2}\right], \tag{10}$$

$$w_{a,t}^2 = (1-\varepsilon^2)w_{b,t}^2. \tag{11}$$

To mitigate the effects of nonzero eccentricity, it is necessary to manage dispersion such that the dispersion along the y-direction is slower than that along the x-direction by a factor of $(1-\varepsilon^2)$. This can be experimentally achieved by introducing a weak 2D optical lattice (OL) along with the elliptical waveguide [40, 56] with their lattice vectors satisfying $\frac{k_x}{k_y} = \sqrt{1-\varepsilon^2}$ [57, 58]. Moreover, the influence of ellipticity can be counteracted by adjusting the depth of the elliptical waveguide. The impact of varying width along the circumference can be nullified by modulating the waveguide's depth.

III. DISPERSION MANAGEMENT OF GROUND STATES

After incorporating the appropriate dispersion management, the effective Gross-Pitaevskii equation becomes [40, 56, 59–64]:

$$i\frac{\partial\psi}{\partial t} = \left[-\frac{\alpha}{2}\frac{\partial^2}{\partial x^2} - \frac{\beta}{2}\frac{\partial^2}{\partial y^2} + g|\psi|^2 + V(x,y)\right]\psi. \tag{12}$$

Here, α and β are the dispersion coefficients in x- and y-directions, respectively, whereas $V(x, y)$ is the potential of the elliptical waveguide.

Numerical Method: The ground state solution of Eq.[12] is numerically obtained by implementing the imaginary time propagation (ITP) method, where the initial wavefunction is allowed to evolve in imaginary time, $t = i\tau$. In this case, any initial wavefunction under the action of time evolution operator, $\exp(-\tau\hat{H})$, asymptotically converges to the ground state solution as $t \to \infty$ [65]. The time dynamics of a localized matter wave packet in the elliptical waveguide are obtained by the real time propagation (RTP) method. In both ITP and RTP methods, the linear and non-linear parts of the dynamical equation are treated separately, where the linear part is evolved in the momentum space, and the non-linear part is evolved in the coordinate space [66]. The x and y coordinates are equally divided into 512 grids with a step size of 0.1. The step size for time is 0.08, totalling 16384 grids. In our work, we have considered ^{23}Na BEC of $N = 1000$ atoms, with parameters $m = 3.816 \times 10^{-26}$ kg, $\omega_\perp = 512$ Hz, $a_\perp = 2.318\mu$m, and $a_s = 2.75 \times 10^{-9}$m [55, 67, 68]. The initial condensate in the form of binary peaks is placed diametrically opposite along the x-axis with the coordinates $(a, 0)$ and $(-a, 0)$, respectively.

A. Ground State of BEC in an Elliptical Waveguide

For numerically finding the ground states, we consider a circular waveguide of radius $a = 10a_\perp$ and unity dispersion coefficients ($\alpha = \beta = 1$), for which the ground state density is uniform along the ring's circumference. Figure 2(a) shows the ground state of the circular waveguide. The solution can be expressed as follows:

$$\psi_c(x,y) = \left(\frac{\sqrt{V_0}}{\pi\gamma}\right)^{\frac{1}{4}} e^{-\frac{\sqrt{V_0}(\sqrt{x^2+y^2}-a)^2}{2\gamma}}, \tag{13}$$

The ground state of the potential is a Gaussian ring since the cross-section of the potential in the vicinity of the minima is harmonic in nature. Such Gaussian ring condensate inside a circular waveguide has been discussed in various experimental and theoretical works [30, 69]. More interesting things happen when we increase the eccentricity of the ring waveguide from null. The stationary states for waveguides with various eccentricities are shown in Fig.2(b-e). The density is no longer uniformly distributed across the circumference of the waveguide, whereas one could see the density accumulation at the semi-major edges. The greater the eccentricity, the

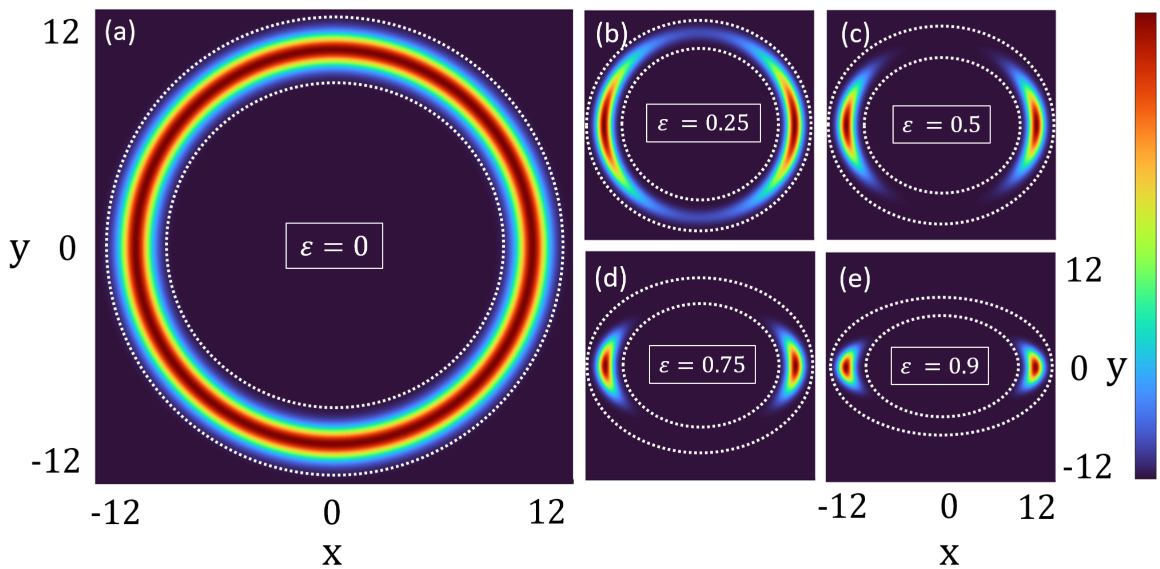

FIG. 2. Ground State solution of BEC in (a) a circular waveguide, $\varepsilon = 0$ and elliptical waveguides of eccentricity (b) $\varepsilon = 0.25$, (c) $\varepsilon = 0.5$, (d) $\varepsilon = 0.75$ and (e) $\varepsilon = 0.9$. The circular ring radius and the semimajor radius are taken as $a = 10a_\perp$. x and y are in the units of $a_\perp = 2.32\ \mu$m and, t is in the units of $1/\omega_\perp = 1.95$ ms.

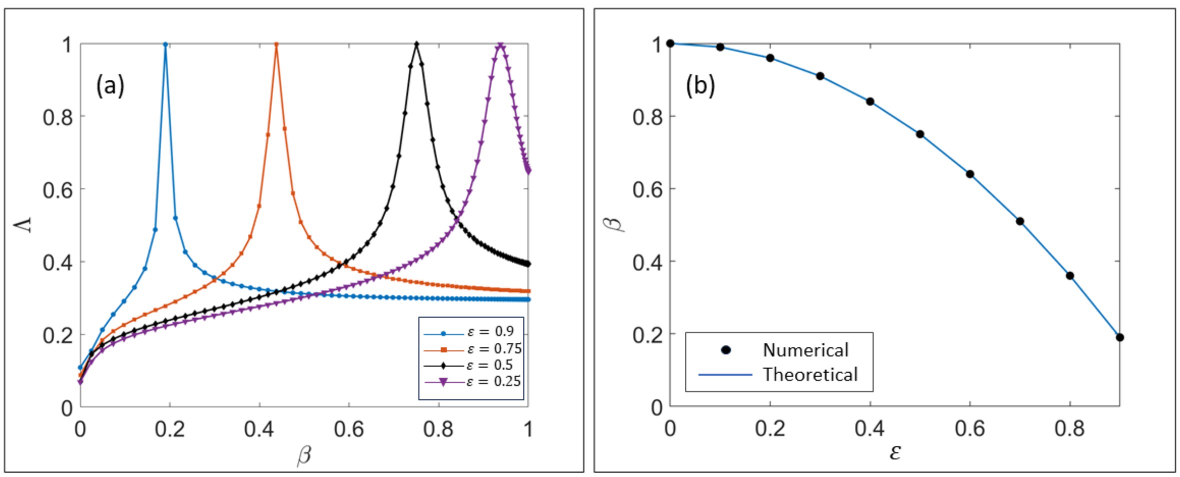

FIG. 3. (a) Variation of overlap of the actual and desired wavefunction with the dispersion coefficient for various values of eccentricities. Solid lines with circles, squares, diamonds and triangles represent the eccentricities $\varepsilon = 0.9$, $\varepsilon = 0.75$, $\varepsilon = 0.5$ and $\varepsilon = 0.25$, respectively. (b) Numerical (dot) and theoretical (solid line) values of dispersion coefficient for various eccentricities. The circular ring radius and the semimajor radius are taken as $a = 10a_\perp$.

greater the density accumulation at the edges, thereby making the waveguide behave like a double-well potential. If the curvature effects are counterbalanced, one could obtain a uniform stationary state in an elliptical waveguide, expressed quite similar to Eq.13:

$$\psi_e(x,y) = Ae^{-\frac{\sqrt{V_0}\left(\sqrt{x^2+\frac{y^2}{1-\varepsilon^2}}-a\right)^2}{2\gamma}}. \tag{14}$$

B. Coefficients of Dispersion to Obtain Uniform Stationary State

As we increase the eccentricity of the waveguide, it gradually transforms to an effective double-well potential, resulting into a non-uniform stationary state along the circumference. As discussed earlier, to eliminate the effects of nonzero eccentricities, we employ the method of dispersion management. The dispersion coefficients, α and β, are tuned and here, we keep $\alpha = 1$ and vary

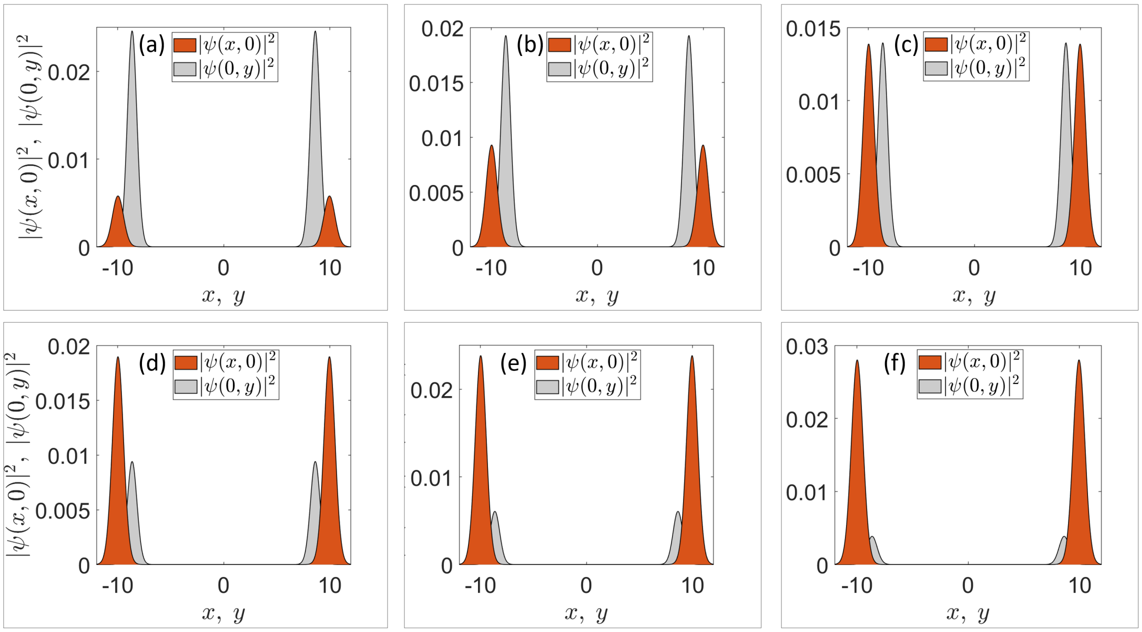

FIG. 4. 1D Cross-Sectional Densities in x and y directions for various β values (a) 0.7250, (b) 0.7375, (c) $0.75 = \beta_c$, (d) 0.7625, (e) 0.7750, (f) 0.7875. The circular ring radius and the semimajor radius are taken as $a = 10a_\perp$. x and y are in the units of $a_\perp = 2.32\ \mu$m and, t is in the units of $1/\omega_\perp = 1.95$ ms.

β to obtain a uniform stationary state in the elliptical waveguide. For the purpose of determining β, we find the overlap of the condensate density with an expected uniform density given in Eq.14. The overlap between these two wavefunctions is defined by,

$$\Lambda = \frac{[\int_{-\infty}^{\infty}\int_{-\infty}^{\infty}|\psi_e(x,y)|^2|\psi_a(x,y)|^2 dxdy]^2}{\int_{-\infty}^{\infty}|\psi_e(x,y)|^4 dxdy\int_{-\infty}^{\infty}|\psi_a(x,y)|^4 dxdy}. \tag{15}$$

Here, $\psi_e(x,y)$ is the expected wavefunction given in Eq.14 and $\psi_a(x,y)$ is the actual wavefunction obtained numerically. Hence, unity overlap function ($\Lambda = 1$) will imply uniform distribution of condensate density along the perimeter of the waveguide, whereas lower values of Λ indicate deformations. Figure 3(a) shows the variation of the overlap function with β for different eccentricities. The maxima in the Λ *vs* β curves will give us the necessary β_c values to get the uniform ground state inside an elliptical waveguide. It is worth observing that, β_c becomes lower for higher eccentricities.

C. Dispersion Coefficients and Eccentricities

We have noticed that, for higher eccentricity one needs to take lower β_c to maintain the uniformity of the ground state. However, the exact relationship between β_c and eccentricity is not obtained. To obtain this relation, we write Eq. 12 with the transformed variable, $Y = \frac{y}{\sigma}$, where $\sigma = \sqrt{1-\varepsilon^2}$:

$$\left[i\frac{\partial}{\partial t} + \frac{\alpha}{2}\frac{\partial^2}{\partial x^2} + \frac{\beta}{2\sigma^2}\frac{\partial^2}{\partial Y^2} - g|\psi|^2 - V(x,Y)\right]\psi = 0,$$

where $\psi \equiv \psi(x,Y)$. The potential of the elliptical waveguide transforms to

$$V(x,Y) = V_0\left[1 - e^{-\frac{1}{\gamma^2}(\sqrt{x^2+Y^2}-a)^2}\right]. \tag{16}$$

Therefore, it becomes transparent to infer that, the dynamical equations for circular and elliptic cases take identical form provided

$$\frac{\beta_c}{\alpha_c} = 1 - \varepsilon^2. \tag{17}$$

This confirms the earlier prediction from the width dynamics of a Gaussian wavepacket in the vicinities of semi-major and semi-minor edges. The obtained β_c is plotted along with it numerically obtained values in Fig.3(b), where the dots indicate the numerical values and the solid line indicates the values obtained from Eq.17. It is clear that β_c falls as we increase the eccentricity, such that $\beta_c = 1$ for a circular waveguide and $\beta_c \to 0$ for higher eccentricities. The desired dispersion coefficient β_c, being a maximum in the overlap Λ, indicates that the ground state density below and above β_c must be non-uniformly distributed and different from each other. This is visualized in Fig. 4 to find the cross-sectional

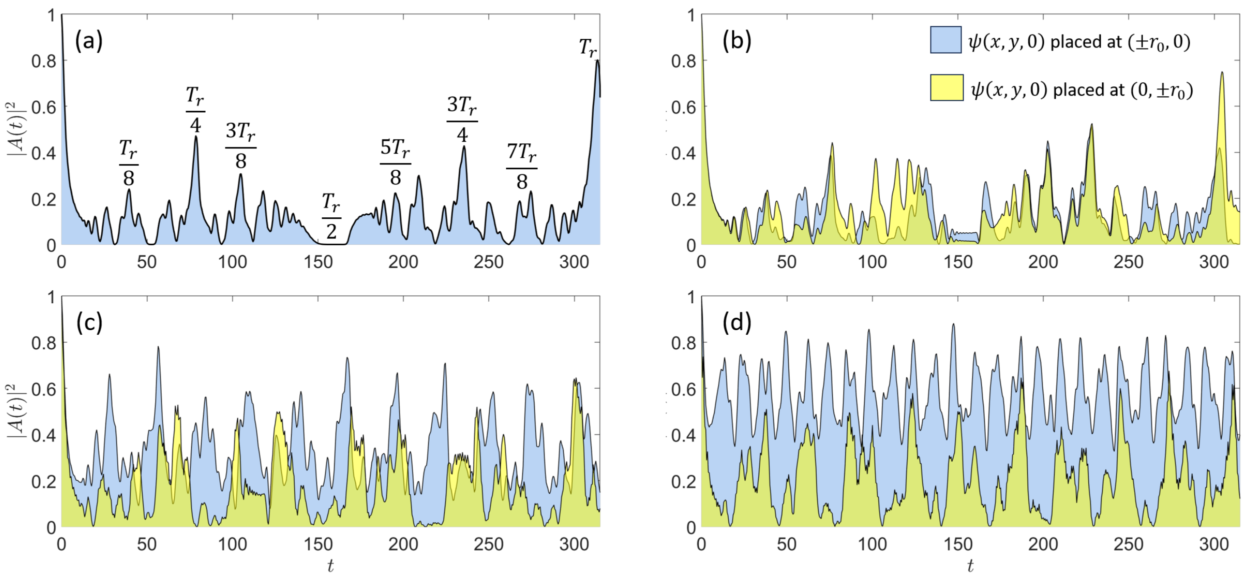

FIG. 5. Survival function for two different initial orientations of the initial clouds $(\pm a, 0)$ and $(0, \pm a)$, with interatomic interaction $g = 2$ and, for eccentricities (a) $e = 0$, (b) $e = 0.25$, (c) $e = 0.75$ and (d) $e = 0.9$. The circular ring radius and the semimajor radius are taken as $a = 10a_\perp$. t is in the units of $1/\omega_\perp = 1.95$ ms.

densities in the elliptical ring along the semi-major and semi-minor axes. The 1D cross-sectional (CS) densities along the semi-major and semi-minor axes are denoted by $|\psi(x, 0)|^2$ and $|\psi(0, y)|^2$, respectively. Figure 4 is depicted for a variety of eccentricities, where it is clear that at $\beta = \beta_c = 0.75$, as shown in Fig.4(c), the 1D cross-sectional densities along the semi-major and semi-minor axis are almost equal, $|\psi(x, 0)|^2 \approx |\psi(0, y)|^2$. On the other hand, for $\beta < \beta_c$, $|\psi(x, 0)|^2 < |\psi(0, y)|^2$ (see Fig.4(a-b)) and for $\beta > \beta_c$, $|\psi(x, 0)|^2 > |\psi(0, y)|^2$ (see Fig.4(d-f)). Without any dispersion management, the dispersion coefficient is unity, $\beta = 1$, corresponding to the complete density accumulation at the semi-major edges and $|\psi(0, y)|^2 \approx 0$.

IV. FRACTIONAL REVIVALS IN AN ELLIPTICAL WAVEGUIDE AND DISPERSION MANAGEMENT

When a localised cloud of BEC is placed in a circular waveguide, it disperses and interferes with itself, forming interference fringes. The time at which the interference brings out the revival of the dispersed cloud in shape and position is termed the revival time T_r. At fractional multiples of the revival time, we can have multiple replicas of the initial condensate. This phenomenon is called fractional revivals. In this work, the initial condensate in the form of binary peaks is placed at $(\pm a, 0)$. From the physics of dispersion, the revival time and FR time scales of two clouds in a circular waveguide of circumference, $C = 2\pi r_0$, are given by [32]

$$T_r = \frac{C^2}{4\pi}, \quad t = \frac{p}{q} T_r, \tag{18}$$

where p and q are mutually prime integers. However, things are different when one places the binary peaks of BEC inside an elliptical waveguide of high eccentricity.

A. Revival Time Scale for an Elliptical Waveguide

The revival dynamics are conventionally studied by the time-dependent characteristic functions such as the autocorrelation function $A(t)$ or the survival function $S(t)$ [70–72]. The survival function is the probability of finding the condensate in its initial state. In other words, it is the absolute square of the Autocorrelation function $A(t)$, which is defined as follows:

$$S(t) = |A(t)|^2, \tag{19}$$

$$A(t) = \int_{-\infty}^{\infty} \int_{-\infty}^{\infty} \psi^*(x, y, 0)\psi(x, y, t) dx dy. \tag{20}$$

It is a time series that quantifies the overlap of the wavefunction at a later time with that of the initial wavefunction, where its value closer to 1 indicates full revival, and the smaller peaks indicate FR instances. In a circular waveguide, at half revival $T_r/2$ and its odd integral multiples, $|A(t)|^2$ becomes zero since the clouds are at position $(0, \pm a)$, which is spatially orthogonal to the initial location $(\pm a, 0)$. Figure 5 shows the survival function $|A(t)|^2$ for BEC in an elliptical waveguide of differ-

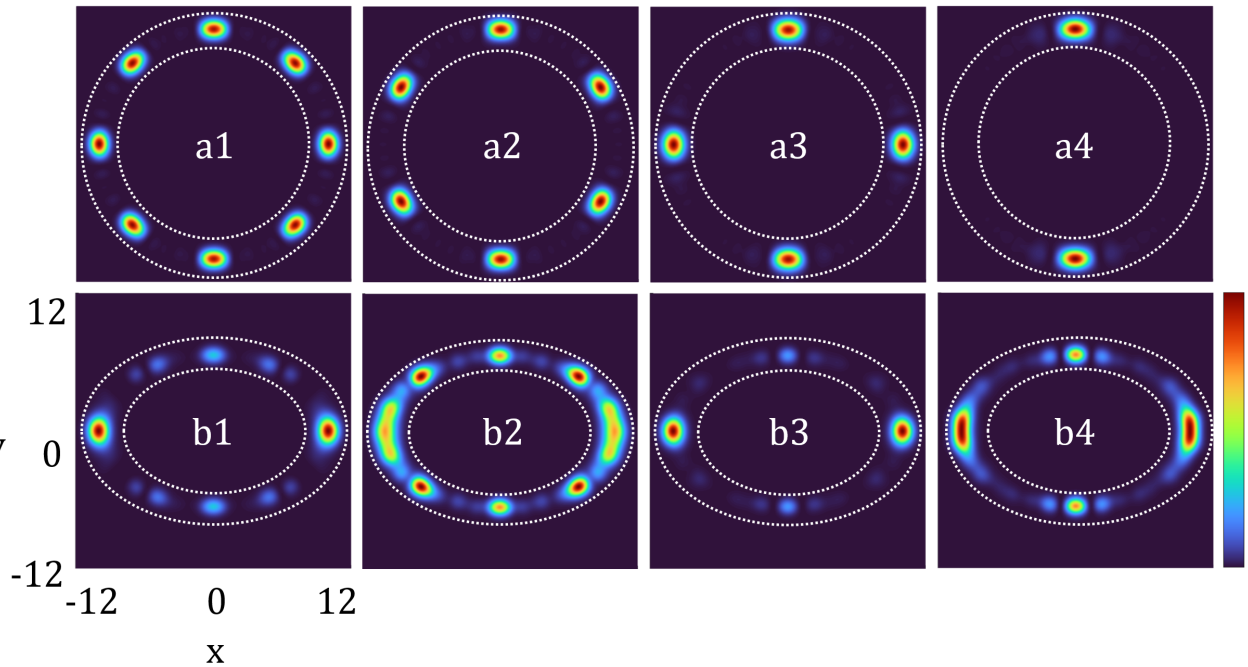

FIG. 6. Condensate density in circular waveguide $\varepsilon = 0$ at time instances 20.14 ms, 26.85 ms, 40.28 ms and 80.57 ms shown in a1, a2, a3 and a4, respectively. Condensate density in an elliptical waveguide of eccentricity $\varepsilon = 0.75$ at time instances 14.50 ms, 19.30 ms, 28.95 ms and 57.90 ms shown in b1, b2, b3 and b4, respectively. The circular ring radius and the semimajor radius are taken as $a = 10a_\perp$. x and y are in the units of $a_\perp = 2.32$ μm and, t is in the units of $1/\omega_\perp = 1.95$ ms.

ent eccentricities (a) $\varepsilon = 0$, (b) $\varepsilon = 0.25$, (c) $\varepsilon = 0.75$, and (d) $\varepsilon = 0.9$. Here, one could note that for $\varepsilon = 0$, there is a clear signature of FR, as pointed out in Fig. 5 (a). However, the signature of FR disappears at higher eccentricities. At eccentricity as high as $\varepsilon = 0.9$, one could see many peaks with similar heights and the minimum of the survival function no longer touches zero, indicating that the cloud spends most of its time at the semi-major edges $(\pm a, 0)$. This is delineated by showing the survival function for two different initial orientations of the clouds, namely $(\pm a, 0)$ and $(0, \pm a)$, in Fig.5. At $\varepsilon = 0$, the survival functions coincide for these two different orientations, whereas at higher eccentricities, the survival functions are no longer identical. While the survival function for $(0, \pm a)$ orientation touches zero more often, the survival function for $(\pm a, 0)$ orientation hardly touches zero. Therefore, irrespective of where the initial clouds are placed inside the elliptical waveguide, the cloud tends to spend most of its time in the semi-major edges. This clearly indicates the disruption of FR instances in an elliptical waveguide. However, one would still get FR instances at very low eccentricities, and the corresponding time scales are worth finding out.

B. Restoration of Fractional Revivals through Dispersion Management

When the eccentricity of the waveguide is non-zero, the revival time takes the form,

$$T_r = \frac{a^2[\int_0^{2\pi} \sqrt{1 - \varepsilon^2 \sin^2 \phi} d\phi]^2}{4\pi}, \tag{21}$$

since the circumference of an ellipse is given by,

$$C = a \int_0^{2\pi} \sqrt{1 - \varepsilon^2 \sin^2 \phi} d\phi, \tag{22}$$

where $\phi \in [0, 2\pi]$ is the azimuthal coordinate, and a, b are semi-major and semi-minor radii, respectively.

At low eccentricities, the daughter condensates of the FR are spatially resolved, and the revival time can be defined by Eq.21. However, at higher eccentricities, the multiple splits of the FR are no longer spatially resolved, and the FR patterns are disrupted. This is evident from Fig. 6, where the condensate densities at times $\frac{T_r}{8}$, $\frac{T_r}{6}$, $\frac{T_r}{4}$, and $\frac{T_r}{2}$ are denoted by numbers 1, 2, 3, 4, respectively. Figures for the two distinct cases ($\varepsilon = 0$ and 0.75) are consequently leveled by (a) and (b). One can observe no-FR for $\varepsilon = 0.75$ and the cloud tends to spend more time at the semi-major edges, irrespective of the initial placement of the cloud. In the previous section, we showed that choosing the appropriate dispersion coef-

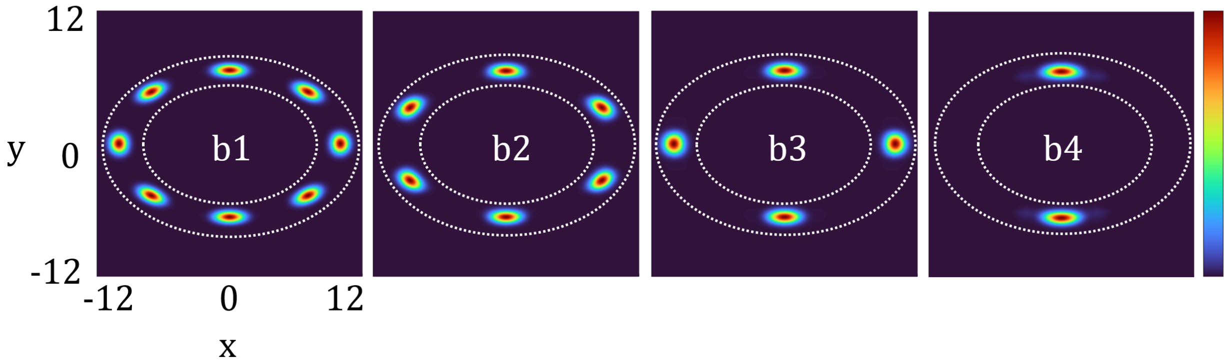

FIG. 7. Snapshots of DM condensate density in elliptical waveguide of eccentricity $\varepsilon = 0.75$ at time instances 20.14 ms, 26.85 ms, 40.28 ms and 80.57 ms shown in b1, b2, b3 and b4, respectively. The semimajor radius is $a = 10a_\perp$. x and y are in the units of $a_\perp = 2.32$ μm and, t is in the units of $1/\omega_\perp = 1.95$ ms.

Eccentricity	$\varepsilon = 0$	$\varepsilon = 0.25$	$\varepsilon = 0.75$	$\varepsilon = 0.9$
T_r before DM (ms)	161.10	156.07	115.80	95.86
T_r after DM (ms)	161.10	161.10	161.10	161.10

TABLE I. Revival time for different eccentricities before and after dispersion management. The circular ring radius and the semimajor radius are taken as $a = 10a_\perp$.

ficients could nullify the effects of the non-constant curvature and produce uniformly distributed ground states inside an elliptical waveguide. We apply this technique to restore fractional revivals of matter waves in an elliptical waveguide. We choose the dispersion coefficients $\alpha = 1$ and $\beta = 1 - \varepsilon^2$, as obtained in Eq. 17. The spatial resolution of the daughter condensates at FR instances, for $\varepsilon = 0.75$, is far lower than that in $\varepsilon = 0.5$. In such a case, the significance of dispersion management is greatly evident. Figure 7 shows the snapshots of dispersion managed condensate density for eccentricity $\varepsilon = 0.75$ at FR instances $\frac{Tr}{8}$, $\frac{Tr}{6}$, $\frac{Tr}{4}$ and, $\frac{Tr}{2}$ denoted by $b1$, $b2$, $b3$ and, $b4$, respectively. The snapshots confirm the restoration of FR patterns of dispersion-managed BEC in an elliptical waveguide. The daughter condensates at the FR instances are spatially resolved in the case of dispersion-managed BEC. Interestingly, for a dispersion-managed matter wave, the revival time and FR times no longer depend on the eccentricity, unlike the non-dispersion-managed case. Table I shows the revival times for different eccentricities without and with dispersion management (DM). One could note that after DM, the BEC revives at times independent of the eccentricity of the waveguide. The eccentricity-dependent dispersion coefficient (Eq.17) balances the eccentricity-dependent time scale (Eq.21) of the matter wave. In other words, the ellipticity-induced effects are nullified through dispersion management, and the matter-wave in the elliptical waveguide of semi-major radius a behaves like that in a circular waveguide of radius a.

V. CONCLUSION

We investigated the influence of ellipticity on the ground state of a BEC within an elliptical waveguide and its impact on the FR instances in a localized matter wave. The elliptical waveguide exhibits behaviour reminiscent of a double-well potential. Notably, an increase in eccentricity correlates with a heightened concentration of condensate density at these semi-major edges. We effectively manage dispersion to counteract the effects of variable thickness within the elliptical waveguide. We achieve a uniform ground state by identifying optimal dispersion coefficients from the overlap function. Interestingly, these coefficients are found to be contingent upon the waveguide's eccentricity.

In the subsequent phase of our investigation, we explore the disruption of FR patterns in a localized matter wave confined within an elliptical waveguide. We employ the time-dependent characteristic function known as the survival function to analyze the perturbed dynamics of the FR instances. Further, using the determined dispersion coefficients, we restore the FR instances of the Bose-Einstein condensate within the elliptical waveguide. This comprehensive study sheds light on the intricate interplay between ellipticity and dispersion of matter waves and offers exchanging the physical merits between the atomtronics applications with zero and non-zero eccentricities.

VI. ACKNOWLEDGEMENT

LS is partially supported by the European Union-NextGenerationEU within the National Center for HPC, Big Data and Quantum Computing [Project No. CN00000013, CN1 Spoke 10: Quantum Computing], by the BIRD Project Ultracold atoms in curved geometries of the University of Padova, by Iniziativa Specifica Quantum of Istituto Nazionale di Fisica Nucleare, by the European Quantum Flagship Project PASQuanS 2, and by the PRIN 2022 Project Quantum Atomic Mixtures: Droplets, Topological Structures, and Vortices, and by the Project Frontiere Quantistiche within the 2023 funding programme 'Dipartimenti di Eccellenza' of the Italian Ministry for Universities and Research. UR acknowledges the support through the project on 'Realistic Exact Model for Quantum Logic Gates and Quantum Computation using Bose-Einstein Condensate' (project No. CRG/2022/007467) by the Science and Engineering Research Board, India.

---

[1] L. Amico, M. Boshier, G. Birkl, A. Minguzzi, C. Miniatura, L.-C. Kwek, D. Aghamalyan, V. Ahufinger, D. Anderson, N. Andrei, *et al.*, "Roadmap on Atomtronics: State of the art and perspective", AVS Quantum Science **3** (2021).

[2] L. Amico, D. Anderson, M. Boshier, J.-P. Brantut, L.-C. Kwek, A. Minguzzi, and W. von Klitzing, "Colloquium: Atomtronic circuits: From many-body physics to quantum technologies", Reviews of Modern Physics **94**, 041001 (2022).

[3] L. Amico, G. Birkl, M. Boshier, and L.-C. Kwek, "Focus on Atomtronics-enabled quantum technologies", New Journal of Physics **19**, 020201 (2017).

[4] C. Ryu and M. G. Boshier, "Integrated coherent matter wave circuits", New Journal of Physics **17**, 092002 (2015).

[5] S. Pandey, H. Mas, G. Vasilakis, and W. von Klitzing, "Atomtronic matter-wave lensing", Physical Review Letters **126**, 170402 (2021).

[6] I. Lesanovsky and W. von Klitzing, "Time-averaged adiabatic potentials: versatile matter-wave guides and atom traps", Physical Review Letters **99**, 083001 (2007).

[7] M. Gildemeister, E. Nugent, B. Sherlock, M. Kubasik, B. Sheard, and C. Foot, "Trapping ultracold atoms in a time-averaged adiabatic potential", Physical Review A **81**, 031402 (2010).

[8] K. Henderson, C. Ryu, C. MacCormick, and M. Boshier, "Experimental demonstration of painting arbitrary and dynamic potentials for Bose-Einstein condensates", New Journal of Physics **11**, 043030 (2009).

[9] S. Pandey, H. Mas, G. Drougakis, P. Thekkeppatt, V. Bolpasi, G. Vasilakis, K. Poulios, and W. von Klitzing, "Hypersonic Bose-Einstein condensates in accelerator rings", Nature **570**, 205 (2019).

[10] P. Navez, S. Pandey, H. Mas, K. Poulios, T. Fernholz, and W. von Klitzing, "Matter-wave interferometers using TAAP rings", New Journal of Physics **18**, 075014 (2016).

[11] J. G. Lee and W. Hill, "Spatial shaping for generating arbitrary optical dipole traps for ultracold degenerate gases", Review of Scientific Instruments **85** (2014).

[12] A. L. Gaunt and Z. Hadzibabic, "Robust digital holography for ultracold atom trapping", Scientific reports **2**, 721 (2012).

[13] S. Gupta, K. Murch, K. Moore, T. Purdy, and D. Stamper-Kurn, "Bose-Einstein condensation in a circular waveguide", Physical review letters **95**, 143201 (2005).

[14] T. A. Bell, J. A. Glidden, L. Humbert, M. W. Bromley, S. A. Haine, M. J. Davis, T. W. Neely, M. A. Baker, and H. Rubinsztein-Dunlop, "Bose-Einstein condensation in large time-averaged optical ring potentials", New Journal of Physics **18**, 035003 (2016).

[15] P. R. Berman, *"Atom interferometry"* (Academic press, 1997).

[16] J. Baudon, R. Mathevet, and J. Robert, "Atomic interferometry", Journal of Physics B: Atomic, Molecular and Optical Physics **32**, R173 (1999).

[17] M. Fattori, C. D'Errico, G. Roati, M. Zaccanti, M. Jona-Lasinio, M. Modugno, M. Inguscio, and G. Modugno, "Atom interferometry with a weakly interacting Bose-Einstein condensate", Physical review letters **100**, 080405 (2008).

[18] J. Petrovic, I. Herrera, P. Lombardi, F. Schaefer, and F. S. Cataliotti, "A multi-state interferometer on an atom chip", New Journal of Physics **15**, 043002 (2013).

[19] R. Sewell, J. Dingjan, F. Baumgärtner, I. Llorente-García, S. Eriksson, E. A. Hinds, G. Lewis, P. Srinivasan, Z. Moktadir, C. O. Gollasch, *et al.*, "Atom chip for BEC interferometry", Journal of Physics B: Atomic, Molecular and Optical Physics **43**, 051003 (2010).

[20] O. Dutta, M. Jääskeläinen, and P. Meystre, "Single-mode acceleration of matter waves in circular waveguides", Physical Review A **74**, 023609 (2006).

[21] T. Haug, R. Dumke, L.-C. Kwek, and L. Amico, "Andreev-reflection and Aharonov-Bohm dynamics in atomtronic circuits", Quantum Science and Technology **4**, 045001 (2019).

[22] S. Ragole and J. M. Taylor, "Interacting atomic interferometry for rotation sensing approaching the Heisenberg Limit", Physical Review Letters **117**, 203002 (2016).

[23] G. Pelegrí, J. Mompart, and V. Ahufinger, "Quantum sensing using imbalanced counter-rotating Bose-Einstein condensate modes", New Journal of Physics **20**, 103001 (2018).

[24] F. Kiałka, B. A. Stickler, and K. Hornberger, "Orbital angular momentum interference of trapped matter waves", Physical Review Research **2**, 022030 (2020).

[25] C. Ryu, P. Blackburn, A. Blinova, and M. Boshier, "Experimental realization of Josephson junctions for an atom SQUID", Physical review letters **111**, 205301 (2013).

[26] A. C. Mathey and L. Mathey, "Realizing and optimizing an atomtronic SQUID", New Journal of Physics **18**, 055016 (2016).

[27] S. Schwartz, M. Cozzini, C. Menotti, I. Carusotto, P. Bouyer, and S. Stringari, "One-dimensional descrip-

tion of a Bose-Einstein condensate in a rotating closed-loop waveguide", New Journal of Physics **8**, 162 (2006).

[28] P. Sandin, M. Ögren, M. Gulliksson, J. Smyrnakis, M. Magiropoulos, and G. Kavoulakis, "Dimensional reduction in Bose-Einstein condensed clouds of atoms confined in tight potentials of any geometry and any interaction strength", Physical Review E **95**, 012142 (2017).

[29] A. Tononi and L. Salasnich, "Low-dimensional quantum gases in curved geometries", Nature Reviews Physics , 1 (2023).

[30] L. Salasnich, "Bose-Einstein condensate in an elliptical waveguide", SciPost Physics Core **5**, 015 (2022).

[31] I. S. Averbukh and N. Perelman, "Fractional revivals: Universality in the long-term evolution of quantum wave packets beyond the correspondence principle dynamics", Physics Letters A **139**, 449 (1989).

[32] J. Bera, S. Ghosh, L. Salasnich, and U. Roy, "Matter-wave fractional revivals in a ring waveguide", Physical Review A **102**, 063323 (2020).

[33] S. Raghav, S. Ghosh, B. Halder, and U. Roy, "Matter Wave Isotope Separation in a Ring Trap", arXiv preprint arXiv:2309.09846 (2023).

[34] P. Pedri, L. Pitaevskii, S. Stringari, C. Fort, S. Burger, F. Cataliotti, P. Maddaloni, F. Minardi, and M. Inguscio, "Expansion of a coherent array of Bose-Einstein condensates", Physical Review Letters **87**, 220401 (2001).

[35] S. Zhang and F. Wang, "Interference effect of three Bose-Einstein condensates", Modern Physics Letters B **16**, 519 (2002).

[36] Z. Hadzibabic, S. Stock, B. Battelier, V. Bretin, and J. Dalibard, "Interference of an array of independent Bose-Einstein condensates", Physical review letters **93**, 180403 (2004).

[37] S. Ashhab, "Interference between a large number of independent Bose-Einstein condensates", Physical Review A **71**, 063602 (2005).

[38] Y. Nikolaieva, L. Salasnich, and A. Yakimenko, "Engineering phase and density of Bose-Einstein condensates in curved waveguides with toroidal topology", New Journal of Physics **25**, 103003 (2023).

[39] A. d. Campo, M. G. Boshier, and A. Saxena, "Bent waveguides for matter-waves: supersymmetric potentials and reflectionless geometries", Scientific reports **4**, 5274 (2014).

[40] B. Eiermann, P. Treutlein, T. Anker, M. Albiez, M. Taglieber, K.-P. Marzlin, and M. Oberthaler, "Dispersion management for atomic matter waves", Physical review letters **91**, 060402 (2003).

[41] J. Su, H. Lyu, and Y. Zhang, "Self-interfering dynamics in Bose-Einstein condensates with engineered dispersions", Physics Letters A **443**, 128218 (2022).

[42] P. Das, A. Khan, and P. K. Panigrahi, "Realization of negative mass regime and bound state of solitons in inhomogeneous Bose-Einstein condensates", The European Physical Journal D **70**, 1 (2016).

[43] P. J. Louis, E. A. Ostrovskaya, and Y. S. Kivshar, "Dispersion control for matter waves and gap solitons in optical superlattices", Physical Review A **71**, 023612 (2005).

[44] G. Barontini and M. Modugno, "Dynamical instability and dispersion management of an attractive condensate in an optical lattice", Physical Review A **76**, 041601 (2007).

[45] M. Khamehchi, K. Hossain, M. Mossman, Y. Zhang, T. Busch, M. M. Forbes, and P. Engels, "Negative-mass hydrodynamics in a spin-orbit–coupled Bose-Einstein condensate", Physical review letters **118**, 155301 (2017).

[46] D. Colas, F. P. Laussy, and M. J. Davis, "Negative-mass effects in spin-orbit coupled Bose-Einstein condensates", Physical Review Letters **121**, 055302 (2018).

[47] B. A. Malomed, *"Soliton management in periodic systems"* (Springer Science & Business Media, 2006).

[48] T. Mayteevarunyoo, B. A. Malomed, and D. V. Skryabin, "Spatiotemporal solitons in dispersion-managed multimode fibers", Journal of Optics **23**, 015501 (2020).

[49] C. J. Pethick and H. Smith, *"Bose-Einstein condensation in dilute gases"* (Cambridge university press, 2008).

[50] L. Pitaevskii and S. Stringari, *"Bose-Einstein condensation and superfluidity"*, Vol. 164 (Oxford University Press, 2016).

[51] F. Dalfovo, S. Giorgini, L. P. Pitaevskii, and S. Stringari, "Theory of Bose-Einstein condensation in trapped gases", Reviews of modern physics **71**, 463 (1999).

[52] S. Adhikari and L. Salasnich, "Localization of a Bose-Einstein condensate in a bichromatic optical lattice", Physical Review A **80**, 023606 (2009).

[53] R. Atre, P. K. Panigrahi, and G. S. Agarwal, "Class of solitary wave solutions of the one-dimensional Gross-Pitaevskii equation", Physical Review E **73**, 056611 (2006).

[54] S. Adhikari, "Vortex-lattice in a uniform Bose-Einstein condensate in a box trap", Journal of Physics: Condensed Matter **31**, 275401 (2019).

[55] N. Murray, M. Krygier, M. Edwards, K. Wright, G. K. Campbell, and C. W. Clark, "Probing the circulation of ring-shaped Bose-Einstein condensates", Physical Review A **88**, 053615 (2013).

[56] B. Eiermann, T. Anker, M. Albiez, M. Taglieber, P. Treutlein, K.-P. Marzlin, and M. Oberthaler, "Bright Bose-Einstein gap solitons of atoms with repulsive interaction", Physical review letters **92**, 230401 (2004).

[57] M. Kraemer, C. Menotti, L. Pitaevskii, and S. Stringari, "Bose-Einstein condensates in 1D optical lattices: compressibility, Bloch bands and elementary excitations", The European Physical Journal D-Atomic, Molecular, Optical and Plasma Physics **27**, 247 (2003).

[58] Z. Liang, X. Dong, Z. Zhang, B. Wu, *et al.*, "Sound speed of a Bose-Einstein condensate in an optical lattice", Physical Review A **78**, 023622 (2008).

[59] N. Z. Petrović, M. Belić, and W.-P. Zhong, "Spatiotemporal wave and soliton solutions to the generalized (3+1)-dimensional Gross-Pitaevskii equation", Physical Review E **81**, 016610 (2010).

[60] A. Al Bastami, M. R. Belić, D. Milović, and N. Z. Petrović, "Analytical chirped solutions to the (3+1)-dimensional Gross-Pitaevskii equation for various diffraction and potential functions", Physical Review E **84**, 016606 (2011).

[61] F. Yu, "Matter rogue waves and management by external potentials for coupled Gross-Pitaevskii equation", Nonlinear Dynamics **80**, 685 (2015).

[62] L. Liu, B. Tian, H.-L. Zhen, X.-Y. Wu, and W.-R. Shan, "Dark and bright solitons for a three-dimensional Gross-Pitaevskii equation with distributed time-dependent coefficients in the Bose-Einstein condensation", Superlattices and Microstructures **102**, 498 (2017).

[63] Q. Liu, "Analytical matter wave solutions of a (2+1)-dimensional partially nonlocal distributed-coefficient

Gross-Pitaevskii equation with a linear potential", Optik **200**, 163434 (2020).

[64] R. Atre and P. K. Panigrahi, "Controlling pulse propagation in optical fibers through nonlinearity and dispersion management", Physical Review A **76**, 043838 (2007).

[65] P. Bader, S. Blanes, and F. Casas, "Solving the Schrödinger eigenvalue problem by the imaginary time propagation technique using splitting methods with complex coefficients", The Journal of chemical physics **139** (2013).

[66] W. Bao and H. Wang, "An efficient and spectrally accurate numerical method for computing dynamics of rotating Bose-Einstein condensates", Journal of Computational Physics **217**, 612 (2006).

[67] K. C. Wright, R. Blakestad, C. J. Lobb, W. D. Phillips, and G. K. Campbell, "Driving phase slips in a superfluid atom circuit with a rotating weak link", Physical review letters **110**, 025302 (2013).

[68] F. Jendrzejewski, S. Eckel, N. Murray, C. Lanier, M. Edwards, C. J. Lobb, and G. K. Campbell, "Resistive flow in a weakly interacting Bose-Einstein condensate", Physical review letters **113**, 045305 (2014).

[69] G. Kavoulakis, "Bose-Einstein condensates with attractive interactions on a ring", Physical Review A **67**, 011601 (2003).

[70] V. Eryomin, S. Vetchinkin, and I. Umanskii, "Manifestations of wave packet fractional revivals in a Morse-like anharmonic system", The Journal of chemical physics **101**, 10730 (1994).

[71] R. W. Robinett, "Quantum wave packet revivals", Physics reports **392**, 1 (2004).

[72] S. Ghosh and J. Banerji, "A time-frequency analysis of wave packet fractional revivals", Journal of Physics B: Atomic, Molecular and Optical Physics **40**, 3545 (2007).